

KCC2 Interacts with the Dendritic Cytoskeleton to Promote Spine Development

Hong Li,¹ Stanislav Khirug,^{2,4} Chunlin Cai,^{2,4} Anastasia Ludwig,¹ Peter Blaesse,² Julia Kolikova,³ Ramil Afzalov,³ Sarah K. Coleman,² Sari Lauri,^{2,3} Matti S. Airaksinen,³ Kari Keinänen,² Leonard Khiroug,³ Mart Saarma,¹ Kai Kaila,^{2,3} and Claudio Rivera^{1,*}

¹Institute of Biotechnology

²Department of Biological and Environmental Sciences

³Neuroscience Center

University of Helsinki, Viikinkaari 4, FIN-00014, Helsinki, Finland

⁴These authors contributed equally to this work.

*Correspondence: claudio.rivera@helsinki.fi

DOI 10.1016/j.neuron.2007.10.039

SUMMARY

The neuron-specific K-Cl cotransporter, KCC2, induces a developmental shift to render GABAergic transmission from depolarizing to hyperpolarizing. Now we demonstrate that KCC2, independently of its Cl⁻ transport function, is a key factor in the maturation of dendritic spines. This morphogenic role of KCC2 in the development of excitatory synapses is mediated by structural interactions between KCC2 and the spine cytoskeleton. Here, the binding of KCC2 C-terminal domain to the cytoskeleton-associated protein 4.1N may play an important role. A more general conclusion based on our data is that KCC2 acts as a synchronizing factor in the functional development of glutamatergic and GABAergic synapses in cortical neurons and networks.

INTRODUCTION

A large number of studies have shown that, during neuronal maturation, GABA_A receptor-mediated responses undergo a change from depolarizing to hyperpolarizing (Ben-Ari, 2002; Payne et al., 2003; Rivera et al., 2005). In cortical neurons, this “developmental shift” is attributable to a change in the expression patterns and functionality of two cation-chloride cotransporters. The Na-K-2Cl cotransporter NKCC1 mediates a Na⁺-dependent active uptake of Cl⁻ that accounts for the depolarizing GABA action in immature neurons (Yamada et al., 2004; Sipila et al., 2006). This is followed by a developmental upregulation of the neuron-specific K-Cl cotransporter KCC2 that is required for hyperpolarizing GABA_A responses (Rivera et al., 1999; Hübner et al., 2001). While the temporal patterns of KCC2 expression have received lots of attention (Payne et al., 2003; Rivera et al., 2005), much less is known about the characteristics and functional significance of the

spatial, subcellular distribution of KCC2 during neuronal maturation.

In cortical neurons, GABAergic synapses are mainly located on the somata and on dendritic regions (shafts) devoid of spines (Freund and Buzsaki, 1996; Somogyi et al., 1998; see also Kubota et al., 2007), while the vast majority of the glutamatergic synapses are formed on dendritic spines (Hering and Sheng, 2001). In view of the key role of KCC2 in GABAergic transmission, it is intriguing that an ultrastructural study showed a remarkable accumulation of KCC2 in the vicinity of asymmetric (glutamatergic) synapses in dendritic spines (Gulyas et al., 2001), suggesting a role for KCC2 that is not directly related to inhibitory transmission.

The formation of dendritic spines is, obviously, a key event in the development of functional glutamatergic synapses (Ethell and Pasquale, 2005; Hering and Sheng, 2001; Yuste and Bonhoeffer, 2004), and it is interesting to note that spinogenesis (Kirov et al., 2004) is closely paralleled by the upregulation of KCC2 in cortical regions (Gulyas et al., 2001; Rivera et al., 2005). These observations point to the existence of shared molecular mechanisms that govern these two major events in neuronal development, hence providing a mechanistic basis for a synchronous maturation of excitatory and inhibitory neurotransmission in cortical neurons and networks.

The rearrangement of the actin cytoskeleton is known to play an important role in spine morphogenesis and structural plasticity both during development and in mature synapses (Ethell and Pasquale, 2005; Matus, 2000). Protein 4.1 is a structural protein that crosslinks the spectrin/actin skeleton with transmembrane proteins (Bennett, 1989; Pinder et al., 1981). Four different isoforms of 4.1 (4.1R, 4.1B, 4.1G, and 4.1N), interacting with a large array of other proteins, have been identified in cells (Denker and Barber, 2002). The mammalian isoform 4.1N was first isolated from brain tissue, and it is known to be expressed in neurons in many parts of the mammalian brain (Walensky et al., 1999; Yamakawa et al., 1999). Notably, this isoform is highly expressed in the postsynaptic density (Scott et al., 1998, 2001) and is thought to be involved in targeting

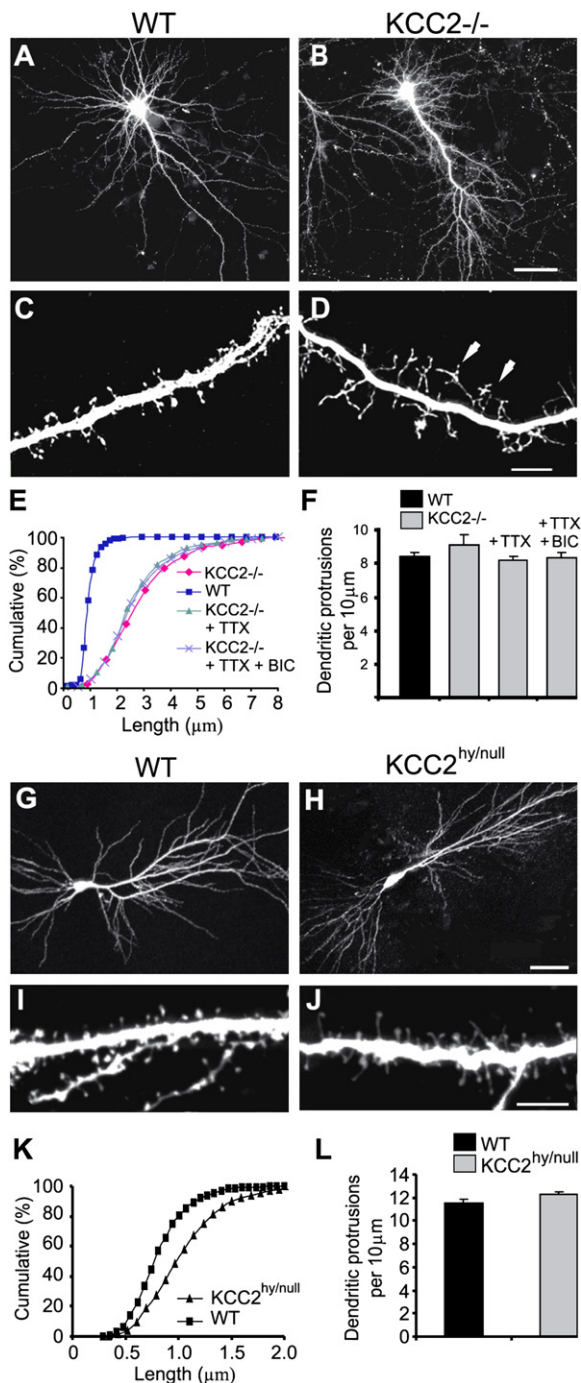


Figure 1. Dendritic Protrusions Are Significantly Longer in *KCC2*^{-/-} than in WT Neurons

Photomicrograph of 14DIV KCC2 WT (A and C) and *KCC2*^{-/-} (B and D) neurons 2 days after transfection with EGFP. High magnification of dendritic regions shows that *KCC2*^{-/-} neurons (D) have significantly longer “filopodia-like” protrusions than the WT (C). (E and F) Cumulative frequency plots of the length (E); $p < 0.001$ and quantification of density (F); $p > 0.2$) of dendritic protrusions in WT and *KCC2*^{-/-} neurons and in *KCC2*^{-/-} neurons cultured in the presence of TTX and TTX plus bicuculline (BIC). Photomicrograph of biocytin-loaded neurons from acute slices from WT (G and I) and *KCC2*^{hy/null} mice (H and J).

and anchoring of synapse-related molecules (Bennett and Baines, 2001; Denker and Barber, 2002), including AMPA-type glutamate receptor subunits (Coleman et al., 2003; Shen et al., 2000).

In this study, we present results showing that KCC2 plays a crucial role in the formation of mature dendritic spines and functional excitatory synapses. A key finding was that maturation of dendritic spines does not take place in the absence of KCC2 expression. Instead, neurons that are devoid of KCC2 develop long dendritic protrusions (up to 5 μm in length) that are branched and highly motile. This is paralleled by a reduction of active synapses, as shown using pre- and postsynaptic markers as well as electrophysiological evidence. Surprisingly, this morphogenic role of KCC2 does not require K-Cl cotransport activity. It is based on a specific structural interaction of KCC2 with the spine cytoskeleton, where the direct binding of the intracellular C-terminal domain of KCC2 with the FERM domain of 4.1N appears to play an important role.

RESULTS

Abnormal Morphology of Dendritic Protrusions in *KCC2*^{-/-} Mice

We first analyzed the morphology of dendritic spines in primary cultures of cortical neurons from *KCC2*-deficient mice (*KCC2*^{-/-}). After 2 weeks in culture (14DIV [days in vitro]), the dendritic protrusions of pyramidal-shaped neurons from *KCC2*^{-/-} mice were remarkably long ($3.84 \pm 0.14 \mu\text{m}$; $n = 2500$ protrusions; 46 neurons; 10 embryos) when compared to wild-type (WT) neurons ($1.53 \pm 0.11 \mu\text{m}$; $n = 1000$ protrusions; 20 neurons; 5 embryos; $p < 0.001$; Figures 1A–1E). Protrusions up to 5 μm long could be observed in the *KCC2*^{-/-} neurons, and their morphology varied from filopodia-like structures (with no obvious spine heads) to protrusions with clear bulbous heads. A number of these protrusions were clearly branched (Figure 1D, arrows), and their emergence and disappearance could be followed in real time using time-lapse confocal microscopy (see Figure S1 and Movies S1 and S2 available online). Notably, the overall density of dendritic protrusions did not differ significantly between *KCC2*^{-/-} ($9.10 \pm 0.58/10 \mu\text{m}$; $n = 65$ dendrites) and wild-type neurons ($8.45 \pm 0.24/10 \mu\text{m}$, $n = 48$ dendrites; $p > 0.2$, Figure 1F).

The formation of aberrant dendritic protrusions in *KCC2*^{-/-} neurons was not attributable to the lack of functional inhibition and consequent neuronal hyperexcitability because an identical phenotype was observed in *KCC2*^{-/-} neurons that were cultured in the continuous presence of TTX (length of protrusions: $3.26 \pm 0.10 \mu\text{m}$; $n = 652$ protrusions; 10 neurons; density of protrusions:

(K and L) Cumulative frequency plot of the length (K); $p < 0.001$ and quantification of density (L); $p > 0.2$) of dendritic protrusions in WT and *KCC2*^{hy/null} neurons. Data are presented as mean \pm SEM. Scale bars: (A, B, G, and H) 50 μm, (C, D, I, and J) 4 μm.

8.01 ± 0.11/10 μm; n = 45 dendrites; 5 embryos; p > 0.1 as compared to *KCC2*^{-/-}; Figures 1E and 1F). In order to study the possible role of GABA_A receptor-mediated transmission (Ganguly et al., 2001), bicuculline (10 μM) was added on top of TTX at 8DIV, i.e., 1 day before the standard time point used for transfection of the neurons by various constructs (see Experimental Procedures). However, blocking GABA_A receptors had no effect on spine morphology as examined at 14DIV (Figures 1E and 1F).

In Vivo Evidence for a Significant Role of KCC2 in the Regulation of Spine Morphology

Next we examined whether the above results are relevant for conditions in vivo. Because it is not possible to address this question with *KCC2*^{-/-} mice, which die immediately after birth (Hübner et al., 2001), we used compound heterozygous mice for *KCC2* null and hypomorphic alleles (*KCC2*^{hy/null}), which express 17% of WT *KCC2* protein levels but are viable (Tomberg et al., 2005). Intracellular biocytin loading in postnatal day (P) 16 acute slices showed that the dendritic protrusions were significantly longer in *KCC2*^{hy/null} neurons (1.21 ± 0.01 μm; n = 1200 protrusions; 8 neurons; 4 mice) than in WT neurons (0.81 ± 0.01 μm; n = 960 protrusions; 6 neurons; 3 mice; p < 0.001; Figures 1G–1K). The increase in dendritic protrusion length was less pronounced than in the *KCC2*^{-/-} neurons. No difference in protrusion density was found between *KCC2*^{hy/null} and WT slices (*KCC2*^{hy/null}: 12.26 ± 0.27/10 μm; n = 51 dendrites; 8 neurons; WT: 11.52 ± 0.31/10 μm; n = 50 dendrites; 6 neurons; p > 0.05; Figure 1L). Furthermore, analysis of spine morphology and density in biocytin-loaded neurons in organotypic slices from *KCC2*^{-/-} cultured for 2 weeks provided similar results as primary cultured neurons (see Figure S2).

The Number of Functional Dendritic Synapses Is Lower in *KCC2*^{-/-} Neurons

Double immunostainings for the presynaptic marker VGLUT1 with either PSD-95 or another postsynaptic marker, HOMER, showed that the density of clusters with both pre- and postsynaptic staining (Kim and Sheng, 2004) was significantly lower in *KCC2*^{-/-} (0.15 ± 0.04 VGLUT1-positive PSD-95 clusters/μm²; 0.18 ± 0.03 VGLUT1-positive HOMER clusters/μm²; n = 7; 4 embryos) than in WT neurons (0.43 ± 0.03 VGLUT1-positive PSD-95 clusters/μm²; 0.51 ± 0.03 VGLUT1-positive HOMER clusters/μm²; n = 7; 4 embryos; p < 0.001; Figures 2A–2D). Taken together, the above structural data are consistent with a reduced number of synapses in *KCC2*^{-/-} neurons.

In order to estimate the density of functionally active synapses, we loaded presynaptic boutons with the styryl dye SynaptoRed C2 for 1 min in the presence of 50 mM KCl (Betz et al., 1992). After washout, the resultant staining was punctuated and consistent with the distribution of synaptic terminals. To confirm that these puncta indeed represented active synaptic boutons, we destained them with a second application of 50 mM KCl in the absence

of SynaptoRed. Only those puncta that were destained by the second KCl application were then counted as active synaptic terminals, and their density was calculated per 10 μm of dendrite length. In control experiments, removal of extracellular Ca²⁺ (with addition of 1 mM EGTA) strongly reduced the density of destained puncta (by 98% ± 1%; n = 7, p < 0.001); furthermore, in the absence of extracellular Ca²⁺ no punctuated SynaptoRed staining was observed, indicating that Ca²⁺-dependent endo- and exocytosis were required for SynaptoRed staining and destaining. The density of destained puncta at dendrites was significantly lower in *KCC2*^{-/-} than in WT neurons (WT: 5.6 ± 0.83/10 μm; n = 10 versus *KCC2*^{-/-}: 2.1 ± 0.52/10 μm; n = 6; p < 0.01) as shown in Figures 2E and 2F. These results show that the number of active presynaptic elements targeting dendrites of *KCC2*^{-/-} neurons is significantly lower than that in WT neurons. No difference in the number of puncta at the somata was observed between WT and *KCC2*^{-/-} neurons (8.12 ± 1.26/soma; n = 4 versus 10.05 ± 3.20/soma; n = 6; p > 0.05; Figures 2E and 2G).

Consistent with the aberrant morphology of dendritic protrusions in the *KCC2*^{-/-} neurons, the above data indicate a prominent reduction in the number of functional synapses. Further evidence supporting this conclusion was obtained by recording excitatory miniature postsynaptic currents (mEPSCs): there was a significantly lower frequency of mEPSCs in *KCC2*^{-/-} neurons (3.5 ± 0.6 Hz; n = 11; p < 0.001) but no difference in amplitude (26.7 ± 1.8 pA; n = 11; p > 0.1) as compared to WT neurons (7.7 ± 0.9 Hz; 25.7 ± 2.1 pA; n = 8; 4 embryos per genotype; Figures 2H–2J).

The Effect of KCC2 on Spine Formation Is Not Dependent on K-Cl Cotransport

GABA_A-mediated depolarization is known to have trophic effects during neuronal development (Akerman and Cline, 2006; Cancedda et al., 2007; Owens and Kriegstein, 2002; Represa and Ben-Ari, 2005). In addition, studies on various cell types have shown that cation-chloride cotransporters can exert a major influence on cell morphology, especially on volume, via actions mediated by changes in the intracellular chloride concentration ([Cl⁻]) (Adragna et al., 2004; Russell, 2000). In order to examine whether a mechanism based on neuronal [Cl⁻] plays a role in the development of spine morphology, we developed a *KCC2* mutant incapable of transporting chloride. The predicted secondary structure for K-Cl cotransporters consists of a short intracellular N-terminal domain followed by 12 transmembrane domains and a large intracellular C-terminal domain (Payne et al., 1996; Figure 3A). Previous work has shown that deletion of the N-terminal domain of the *KCC1* isoform produces a mutant that is not capable of K-Cl cotransport (Casula et al., 2001). We compared full-length (*KCC2*-FL) and the N-terminal domain deletion construct (*KCC2*-ΔNTD) for (1) their efficacy to extrude Cl⁻ and (2) for their ability to restore the dendritic spine phenotype in *KCC2*^{-/-} neurons.

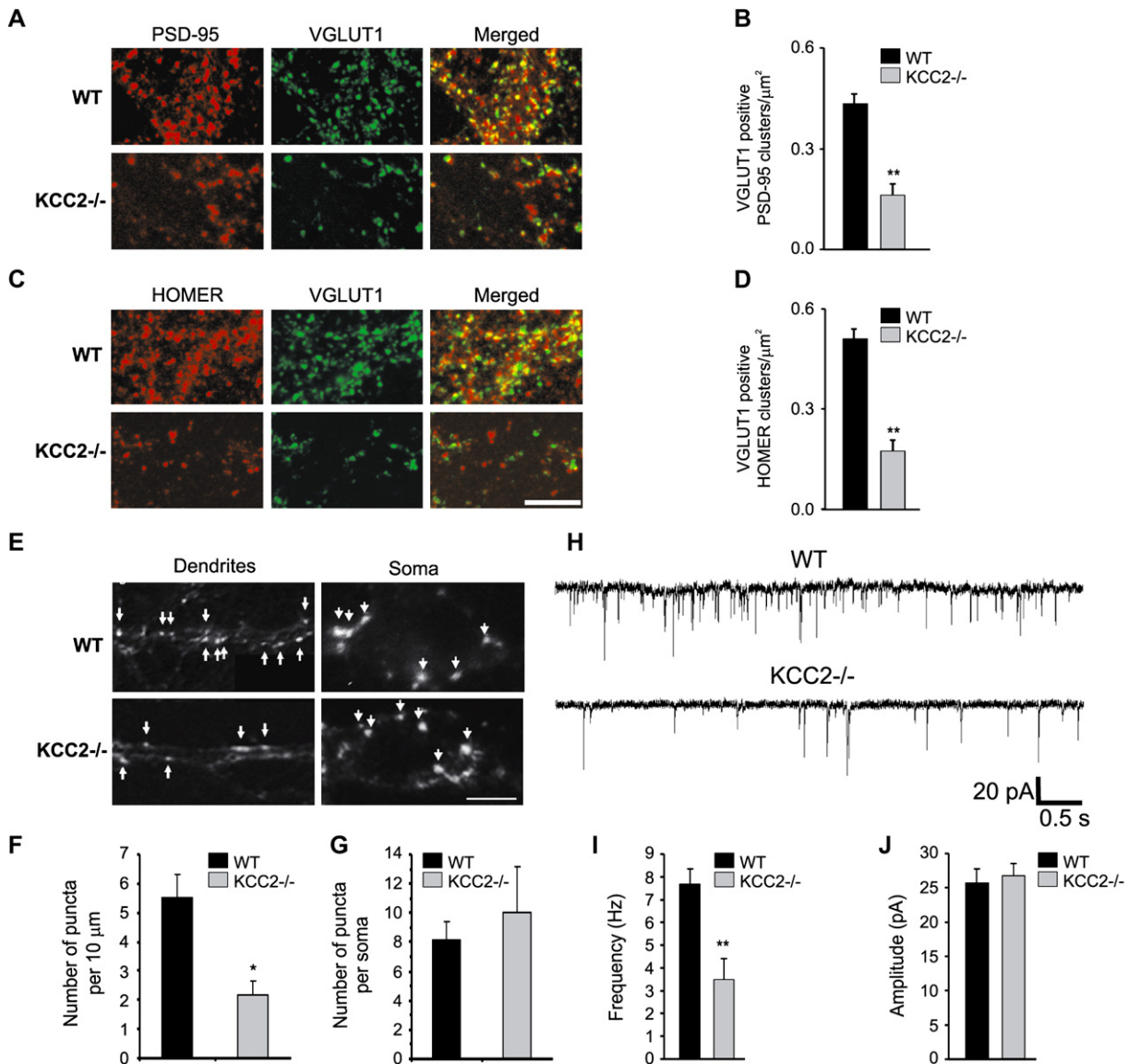


Figure 2. Reduced Number of Functional Synapses in Dendrites of *KCC2*^{-/-} Neurons

Double immunostaining for VGLUT1 and PSD-95 (A) or HOMER (C) of 14DIV WT and *KCC2*^{-/-} neurons. Reduced number of VGLUT1-positive PSD-95 (B) and HOMER (D) clusters in *KCC2*^{-/-} neurons (***p* < 0.001). (E) Active presynaptic terminals in cultured neurons from WT and *KCC2*^{-/-} mice. A significantly lower number of SynptoRed-stained boutons identified as bright spots indicated by arrows is seen in dendrites of *KCC2*^{-/-} neurons, implying a lower number of functional synapses as compared to WT neurons. This difference is only observed in dendrites, not in the somata. Quantification of the number of functional synapses in dendrites (F); **p* < 0.01) and somata (G; *p* > 0.05) of WT and *KCC2*^{-/-} neurons, respectively. (H) Traces showing recordings of mEPSCs in WT and *KCC2*^{-/-} neurons. *KCC2*^{-/-} neurons display a lower frequency (I) but not amplitude (J) of mEPSCs in comparison to WT neurons (***p* < 0.001). Data are presented as mean \pm SEM. Scale bar, (A, C, and E) 5 μm .

The assay of neuronal Cl^- extrusion was based on imposing a somatic chloride load via a whole-cell patch-clamp electrode and measuring the somato-dendritic gradient of the reversal potential of GABA_A receptor-mediated current responses (E_{GABA}) induced along the dendrite by laser flash photolysis of caged GABA (Figure 3A). As described before (Khirug et al., 2005), late embryonic WT neurons that have been cultured for

3–5 days have low expression levels of KCC2 (Ludwig et al., 2003) and a negligible Cl^- extrusion capacity as evidenced by the very small value of the dendritic E_{GABA} gradient ($-0.042 \pm 0.012 \text{ mV}/\mu\text{m}$; *n* = 10; Figure 3B). Notably, following transfection of *KCC2*^{-/-} neurons with KCC2-FL, the E_{GABA} gradient ($-0.17 \pm 0.014 \text{ mV}/\mu\text{m}$; *n* = 6; Figures 3A and 3B) was similar to that in the more mature WT cells (14–22DIV) ($-0.125 \pm 0.019 \text{ mV}/\mu\text{m}$; *n* = 10; Figure 3B)

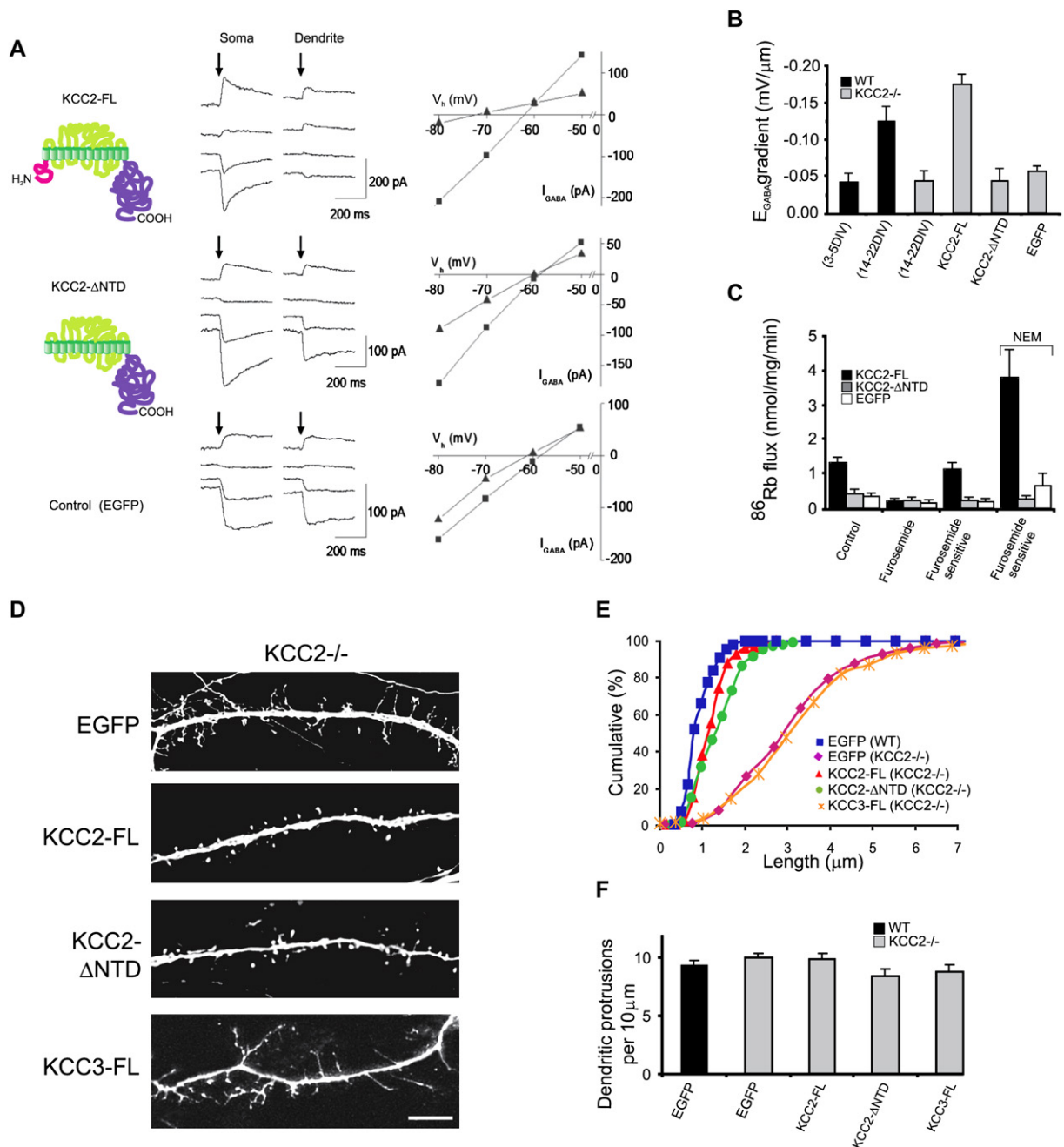


Figure 3. Expression of a KCC2 Mutant, KCC2- Δ NTD, that Is Incapable of K-Cl Cotransport Induces Normal Spine Morphology in KCC2^{-/-} Neurons

The efficacy of K-Cl cotransport mediated by KCC2-FL and KCC2- Δ NTD was determined by estimating their capacity to induce a somatodendritic chloride gradient in WT as well as KCC2^{-/-} neurons. Using somatic patch-clamp and local uncaging of GABA (time point marked by arrow), E_{GABA} was measured in the soma and in dendrites at different distances from the soma (A), and the somatodendritic gradient was calculated (B). Typical traces from GABA_A responses from soma and dendrites are shown with their corresponding I-V plots (A) for KCC2^{-/-} neurons expressing KCC2-FL, KCC2- Δ NTD, and EGFP. (B) A significant developmental increase (3–5DIV to 14–22DIV) in the somatodendritic gradient was found in WT but not in KCC2^{-/-} neurons. KCC2^{-/-} neurons expressing KCC2-FL display a similar gradient as 14–22DIV WT neurons. In contrast, chloride extrusion is not functional in KCC2^{-/-} neurons expressing the KCC2- Δ NTD mutant. (C) K-Cl cotransport measured as furosemide-sensitive ^{86}Rb flux in HEK293 cells transfected with EGFP, KCC2- Δ NTD, or KCC2-FL in the absence and presence of 1 mM N-ethylmaleimide (NEM). The furosemide-sensitive flux in KCC2- Δ NTD-transfected cells was small and not different from that in EGFP-transfected cells and was not significantly stimulated by NEM ($p > 0.2$). (D) Spine morphology in KCC2^{-/-} neurons is rescued by KCC2-FL and KCC2- Δ NTD but not by KCC3-FL. Cumulative frequency plot of dendritic protrusion length (C) and quantification of density of dendritic protrusions (D). Data are presented as mean \pm SEM. Scale bars, (D) 5 μ m.

indicating that overexpression of KCC2-FL in cultured $KCC2^{-/-}$ pyramidal neurons induces effective K-Cl cotransport (Lee et al., 2005; Chudotvorova et al., 2005; Akerman and Cline, 2006).

In striking contrast to the functional data obtained with KCC2-FL, expression of the KCC2- Δ NTD construct in $KCC2^{-/-}$ neurons (see Figure S3) failed to induce K-Cl cotransport. In the $KCC2^{-/-}$ neurons transfected with KCC2- Δ NTD, the E_{GABA} gradient (-0.04 ± 0.016 mV/ μ m; $n = 6$; Figures 3A and 3B) was similar to what was seen in $KCC2^{-/-}$ neurons transfected with EGFP only (-0.057 ± 0.006 mV/ μ m; $n = 4$; Figures 3A and 3B) or not transfected with any construct (-0.044 ± 0.013 mV/ μ m; $n = 9$). In addition to the electrophysiological assays above, we tested the functionality of the constructs using a well-established ^{86}Rb flux assay of K-Cl cotransport in HEK293 cells, where furosemide (a blocker of cation-chloride cotransport) is applied to obtain the baseline values that do not reflect K-Cl cotransport activity (Williams and Payne, 2004) (Figures 3C). In full agreement with the results obtained in neurons, HEK293 cells expressing the KCC2-FL construct induced a pronounced furosemide-sensitive ^{86}Rb flux (1.26 ± 0.18 nmol/mg/min; $n = 3$), whereas cells expressing either KCC2- Δ NTD or EGFP displayed small fluxes that were not significantly above the baseline level (KCC2- Δ NTD: 0.22 ± 0.07 nmol/mg/min; EGFP: 0.20 ± 0.08 nmol/mg/min; $n = 3$). When transport activity was stimulated with NEM, a well-known functional activator of K-Cl cotransport (Williams and Payne, 2004), only the cells that were transfected with KCC2-FL showed a robust increase in the ^{86}Rb flux (Figure 3C) (KCC2-FL: 3.80 ± 0.79 nmol/mg/min; KCC2- Δ NTD: 0.26 ± 0.10 nmol/mg/min; EGFP: 0.65 ± 0.37 nmol/mg/min; $n = 3$).

When we examined the structural effects of ectopic expression of KCC2-FL in $KCC2^{-/-}$ neurons, we found that the neurons displayed normal spine morphology (1.61 ± 0.15 μ m; $n = 1345$ protrusions; 20 neurons) that was not distinguishable from the WT neurons (Figures 3D and 3E). This is an important observation demonstrating that KCC2 overexpression is able to completely rescue the spine phenotype in the $KCC2^{-/-}$ neurons. Surprisingly, however, the nonfunctional KCC2- Δ NTD construct was also able to fully restore normal spine morphology (1.44 ± 0.12 μ m; $n = 1402$ protrusions; 14 neurons; Figures 3D and 3E). Taken together, the data above show that KCC2 promotes spine formation based on a mechanism that is not dependent on functional K-Cl cotransport and that the underlying structural interactions are not mediated by the NTD of KCC2.

In order to gain further information on the specificity of the structural role of KCC2 in spine formation, we transfected $KCC2^{-/-}$ neurons with another K-Cl cotransporter isoform, KCC3 (Payne et al., 2003). Interestingly, the expression of KCC3-FL in $KCC2^{-/-}$ neurons was not able to restore normal spine morphology (Figures 3D and 3E; 3.89 ± 0.18 μ m; $n = 700$ protrusions; 10 neurons). The density of dendritic protrusions was not significantly different between control neurons (EGFP: $9.45 \pm 0.37/$

10 μ m; $n = 40$ dendrites; 17 neurons) and those transfected by any of the four constructs (KCC2-FL: $8.39 \pm 0.63/10$ μ m; $n = 54$ dendrites; 20 neurons; KCC2- Δ NTD: $9.92 \pm 0.49/10$ μ m; $n = 36$ dendrites; 14 neurons; KCC3-FL: $8.76 \pm 0.62/10$ μ m; $n = 20$ dendrites; 10 neurons; EGFP: $9.98 \pm 0.37/10$ μ m; $n = 56$ dendrites; 20 neurons; $p > 0.4$; Figure 3F).

Rescue of Functional Dendritic Synapses in $KCC2^{-/-}$ Neurons by KCC2- Δ NTD

As expected from the results above showing a decrease in the number of functional synapses in $KCC2^{-/-}$ neurons, immunofluorescent staining against PSD-95 in EGFP-expressing neurons showed a significantly lower number of PSD-95-positive protrusions in $KCC2^{-/-}$ as compared to WT neurons (WT: 6.5 ± 0.5 ; $KCC2^{-/-}$: 2.9 ± 0.2 PSD-95-positive protrusions/ 10μ m; $n = 25$ neurons; 6 embryos per genotype; $p < 0.001$; Figures 4A and 4B). In contrast to this, $KCC2^{-/-}$ neurons transfected with the nonfunctional KCC2- Δ NTD construct displayed a significantly higher number of PSD-95-positive protrusions that was close to what was observed in the WT neurons (5.7 ± 0.6 PSD-95-positive protrusions/ 10μ m; $n = 10$ neurons; 3 embryos; EGFP versus KCC2- Δ NTD in $KCC2^{-/-}$, $p > 0.001$; Figures 4A and 4B). In order to further examine the structural requirements needed for the rescue of spines, we tested the effects of transfecting neurons with KCC3-FL. Notably, the number of PSD-95-positive protrusions in neurons expressing KCC3-FL was not different from the EGFP-transfected $KCC2^{-/-}$ neurons (3.2 ± 0.4 PSD-95-positive protrusions/ 10μ m; $n = 10$ neurons; 3 embryos; $p > 0.2$; Figures 4A and 4B). These results indicate that KCC2- Δ NTD has specific structural properties that are needed to restore normal spines carrying PSD-95-positive clusters in $KCC2^{-/-}$ neurons.

In order to assess whether the restored synapses are functionally active, we measured the frequency and amplitude of mEPSCs in $KCC2^{-/-}$ neurons transfected with KCC2- Δ NTD or KCC3-FL and compared these to WT and $KCC2^{-/-}$ neurons transfected with EGFP only. Indeed, the mEPSCs in $KCC2^{-/-}$ neurons expressing KCC2- Δ NTD were not significantly different from WT ($111\% \pm 18\%$ of WT frequency; $n = 8$ neurons; 3 embryos; $p > 0.2$; Figures 4C and 4D). Neurons transfected with KCC3-FL showed a significantly lower frequency, similar to the one found in $KCC2^{-/-}$ neurons transfected with EGFP only (KCC3-FL: $35\% \pm 9\%$ of WT frequency; $n = 6$ neurons; $KCC2^{-/-}$: $32\% \pm 7\%$ of WT frequency; $n = 10$ neurons; $p > 0.001$; Figures 4C and 4D). No difference was found between the amplitudes of mEPSCs in control WT neurons and those transfected with the different constructs (KCC2- Δ NTD: $100\% \pm 6\%$ of WT amplitude; $n = 8$ neurons; KCC3-FL: $85.5\% \pm 19\%$ of WT amplitude; $n = 6$ neurons; $p > 0.2$; Figures 4C and 4E). These results show that synapses restored by KCC2- Δ NTD are functionally active and, notably (see Figure 3), this effect of KCC2- Δ NTD cannot be based on active chloride transport.

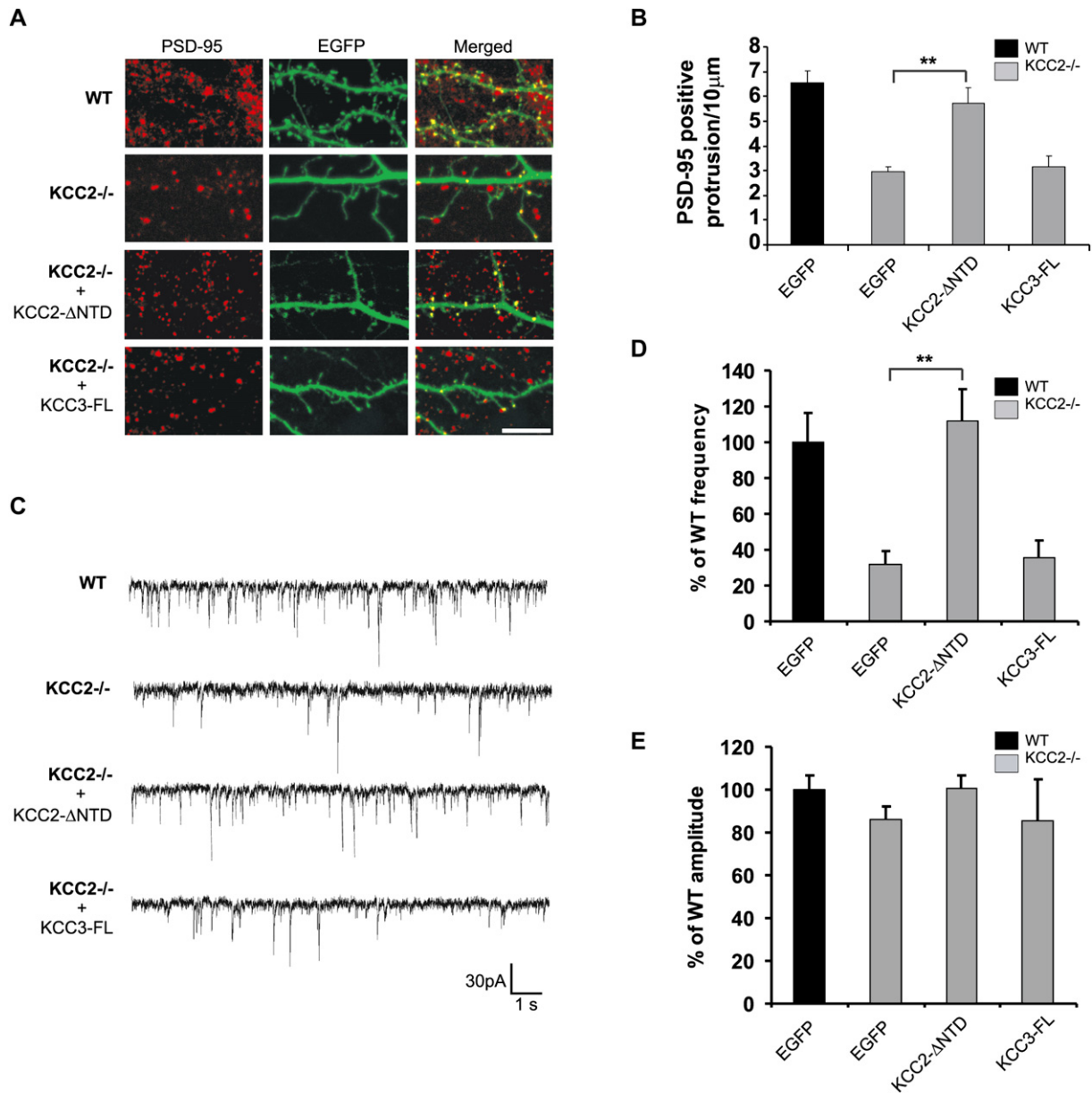


Figure 4. Expression of the Non-Chloride-Extruding KCC2-ΔNTD Restores Functional Synapses in KCC2^{-/-} Neurons

(A) Immunostaining for PSD-95 of WT and KCC2^{-/-} neurons transfected with EGFP, KCC2-ΔNTD, or KCC3-FL. (B) An increased number of PSD-95-positive dendritic protrusions in KCC2^{-/-} neurons transfected with KCC2-ΔNTD (**p < 0.001) but not in neurons transfected with KCC3-FL. (C and D) Electrophysiological recordings showing a significantly higher frequency of mEPSCs in KCC2^{-/-} neurons expressing KCC2-ΔNTD than in neurons expressing EGFP only (**p < 0.001). Expression of KCC3-FL did not affect the frequency of mEPSCs. (C and E) No significant difference in mEPSC amplitude was observed between WT and KCC2^{-/-} neurons transfected with the different constructs. Data are presented as mean ± SEM. Scale bar, (A) 5 μm.

KCC2-CTD Expression Induces Long Dendritic Protrusions

Considering the above results and that the C-terminal domain (KCC2-CTD) is the largest intracellular portion of KCC2, it is plausible to assume that the effect on the morphology of dendritic protrusions could be mediated through the interaction of this domain with other intracel-

lular proteins. We addressed the above question by transfecting cultured WT neurons with a construct containing the KCC2-CTD only (aa 637–1116), with the expectation that it may compete for the interaction with intracellular partners. Notably, when WT neurons were transfected with KCC2-CTD, a significant elongation of dendritic protrusions was found (KCC2-CTD: 2.94 ± 0.18 μm; n = 1682;

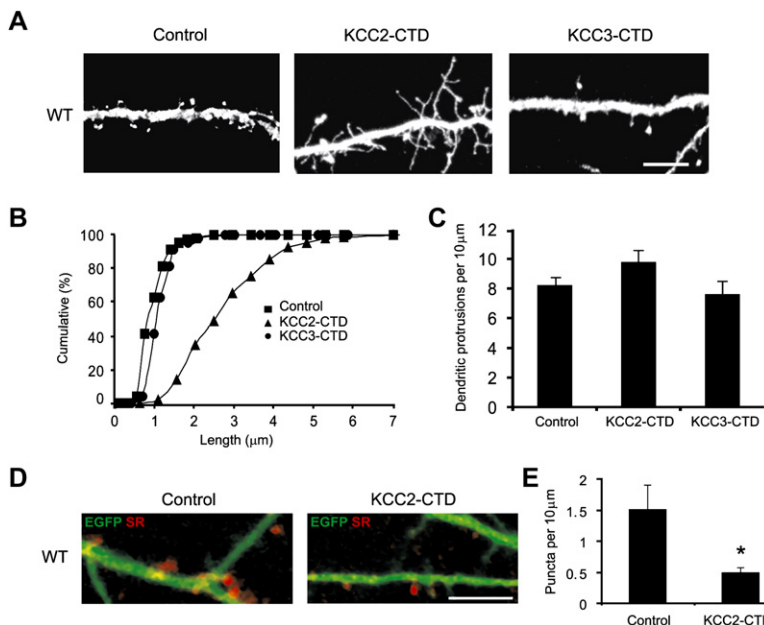


Figure 5. Expression of the KCC2 C-Terminal Domain Induces Filopodia-like Protrusions in Dendrites of WT Neurons

(A) Wild-type neurons transfected with EGFP alone (control), with the pEGFP-IRES-carrying construct for KCC2-CTD expression or EGFP-KCC3-CTD. KCC2-CTD-transfected neurons show long and thin dendritic protrusions very similar to *KCC2*^{-/-} neurons, whereas KCC3-CTD expression does not change the morphology of dendritic protrusion. (B) Cumulative frequency plot of dendritic protrusions in control, KCC2-CTD-, and KCC3-CTD-transfected neurons. (C) Quantification of dendritic protrusion densities ($p > 0.1$). (D) SynptoRed C2 loading in EGFP (control) and KCC2-CTD-expressing neurons. Quantification shows a significantly lower number of functional synapses in the KCC2-CTD-transfected neurons compared to control ($*p < 0.02$) (E). Scale bar, (A and D) 5 μm.

14 neurons versus control: $1.38 \pm 0.14 \mu\text{m}$; $n = 850$; 12 neurons; Figures 5A and 5B), which was both qualitatively and quantitatively very similar to the phenotype of *KCC2*^{-/-} neurons (cf. Figure 1). This effect could be observed soon after transfection (within 2 days) and persisted for the duration of these experiments (5 days). On the contrary, dendritic protrusions in WT neurons transfected with KCC3-CTD were not different from control ($1.41 \pm 0.16 \mu\text{m}$; $n = 510$; 7 neurons; Figures 5A and 5B). No significant change in the number of protrusions was observed in KCC2-CTD- or KCC3-CTD-transfected neurons (Figure 5C). These results indicate that the KCC2-CTD mutant has a dominant-negative effect that leads to the disruption of intracellular interactions that are necessary for normal dendritic spine morphogenesis. This conclusion gained further support from experiments that showed that the number of active presynaptic boutons loaded with SynptoRed was significantly lower in KCC2-CTD-expressing neurons as compared with control neurons (control: $1.52 \pm 0.39/10 \mu\text{m}$; $n = 3$ versus KCC2-CTD: $0.50 \pm 0.07/10 \mu\text{m}$; $n = 4$; $p < 0.01$; Figures 5D and 5E).

The Cytoskeleton-Associated Protein 4.1N Interacts with KCC2

Dendritic spines are the main target of excitatory synapses, containing a variety of glutamate receptors, signaling molecules, and scaffold proteins in conjunction with an actin-rich cytoskeleton (Hering and Sheng, 2001; Ethell and Pasquale, 2005). To find out the interacting partners of KCC2 within spines, we screened antibodies against glutamate receptor subunits (GluR1–4) and other proteins enriched in spines (Kennedy et al., 2005; Niethammer et al., 1998; Shen et al., 2000), including PSD-95, GRIP, CaMKII, CRIPT, SAP97, and 4.1N, using KCC2 immuno-

precipitation assays from adult mouse brain homogenate. Out of these, the antibody against the cytoskeleton-interacting protein 4.1N was the only one capable of precipitating KCC2 (Figure 6A and Figure S4).

Actin filaments within the dendritic spines are involved in both long-term and short-term changes in spine morphology (Ethell and Pasquale, 2005; Kennedy et al., 2005). 4.1N is a neuronal isoform of the cytoskeleton-associated protein 4.1 family that is known to participate in stabilizing the spectrin/actin cytoskeleton (Hoover and Bryant, 2000; Shen et al., 2000; Walensky et al., 1999). Hence, we went on to further analyze the interaction between 4.1N and KCC2. Coimmunoprecipitation studies using antibodies against both the C-terminal and N-terminal epitopes of KCC2 indicated that 4.1N interacted with KCC2 in the mouse brain homogenate (Figure 6B). Coexpression of KCC2 and Myc-tagged 4.1N in HEK293 cells resulted in a clear Myc-4.1N band in anti-KCC2 immunoprecipitates (Figure 6C). Similarly, the anti-Myc antibody could also bring down KCC2 (Figure 6D). Control transfections using either one of the plasmids alone did not produce any band after blotting (Figures 6C and 6D).

To further identify the molecular domain of KCC2 responsible for the interaction with 4.1N, we transfected HEK293 cells with mutant constructs designed to express two different segments of EGFP-tagged KCC2. The EGFP-KCC2-CTD and KCC2 without the CTD (EGFP-KCC2-ΔCTD) were independently coexpressed with Myc-tagged 4.1N, and their interactions were analyzed by immunoprecipitation. Notably, EGFP-KCC2-CTD, but not EGFP-KCC2-ΔCTD, was able to immunoprecipitate together with Myc-4.1N (Figure 6E). Transfections with any of the plasmids alone were negative. These results show that the KCC2-CTD is responsible for the interaction of KCC2 with 4.1N.

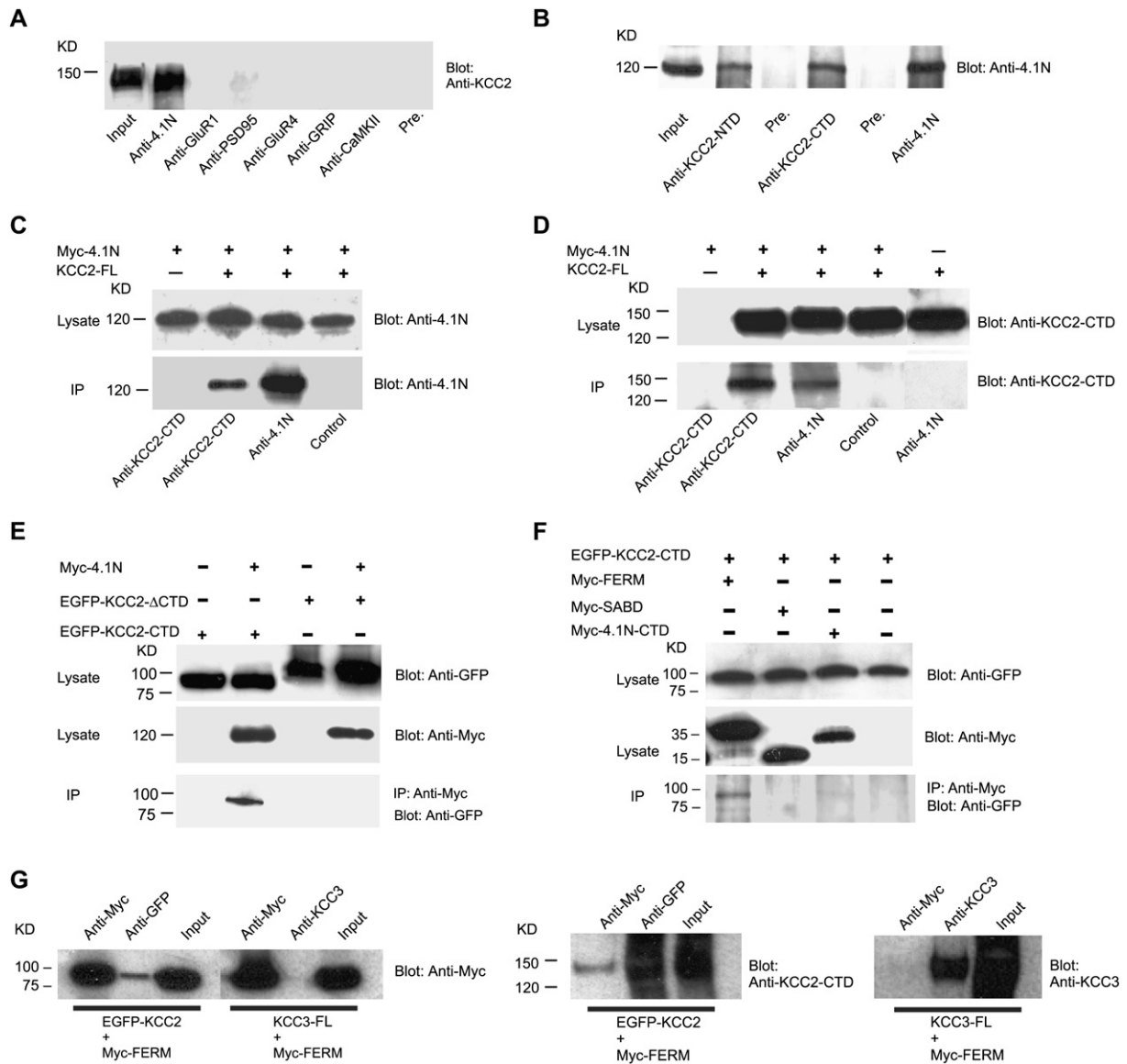


Figure 6. Direct Interaction between KCC2 and 4.1N Demonstrated by Immunoprecipitation

(A) Immunoprecipitation from mouse brain homogenates (input) using antibodies against 4.1N, GluR1, GluR4, PSD-95, GRIP, and CaMKII followed by western blot for KCC2 yielded protein 4.1N as the KCC2 interacting partner. Corresponding preimmune serum (Pre.) was used as control (B). Mouse brain homogenate subjected to immunoprecipitations using antibodies against either the N-terminal or C-terminal domain of KCC2 show clear bands for 4.1N. (C and D) Immunoprecipitation experiments from HEK293 cell homogenates (lysate) coexpressing Myc-4.1N and KCC2. A strong 4.1N band is present in the anti-KCC2 precipitate from coexpressed but not in single expressed cell homogenate (C). (D) The same immunoprecipitations as in (C) were blotted with anti-KCC2 antibody. KCC2 was also brought down by the 4.1N antibody. (E and F) The FERM domain of protein 4.1N binds to the KCC2-CTD. (E) When Myc-tagged 4.1N was coexpressed with either EGFP-KCC2-CTD or EGFP-KCC2-ΔCTD, anti-Myc immunoprecipitates contained EGFP-KCC2-CTD but not EGFP-KCC2-ΔCTD. These results show that 4.1N interacts with KCC2-CTD. (F) Three Myc-tagged domains (FERM, SABD, CTD) of 4.1N were cotransfected with EGFP-KCC2-CTD. Anti-GFP antibody blot after anti-Myc immunoprecipitation shows that only the FERM domain interacts with KCC2-CTD. (G) KCC3-FL does not interact with 4.1N FERM domain. Anti-Myc immunoprecipitates from cells transfected with either EGFP-KCC2-FL or KCC3-FL and Myc-FERM contained only EGFP-KCC2-FL. Deliberate overexposure was used in the right panels to emphasize the lack of interaction between KCC3-FL and the FERM domain of 4.1N.

FERM Domain 4.1N Binds to KCC2 and Induces Long Dendritic Protrusions

To identify the KCC2-CTD binding site in 4.1N, we used Myc-tagged constructs based on three functional do-

maines of 4.1N: FERM, SABD, and 4.1N-CTD (Hoover and Bryant, 2000; Shen et al., 2000). These constructs were coexpressed with the EGFP-tagged KCC2-CTD, and anti-GFP antibodies were used to analyze the Myc

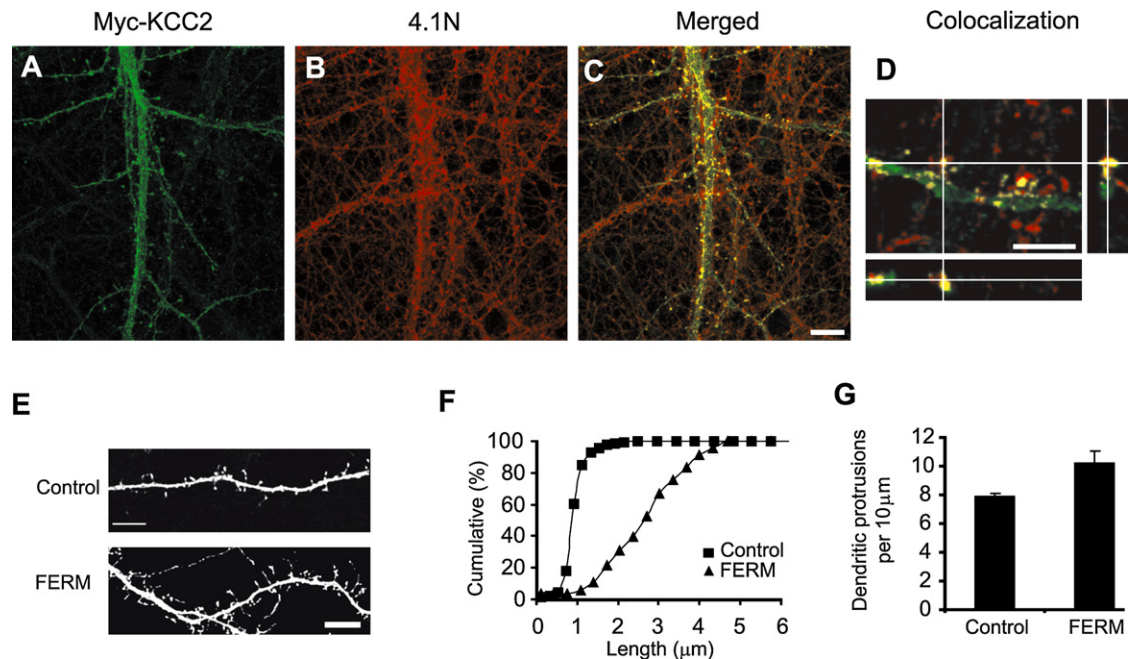


Figure 7. Dominant-Negative Effect of 4.1N FERM Domain on Dendritic Protrusion Morphology

(A) Low-magnification photomicrographs showing the expression of a Myc-KCC2-transfected neuron (green) and (B) the endogenous distribution of 4.1N (red). (C and D) Analysis of the subcellular distribution shows that KCC2 and 4.1N are colocalized (yellow) in dendritic spines (see also Figure S4). (D) High-magnification colocalization analysis using Imaris 4 software. Left and lower panels show the analysis of z sections at the level of the corresponding white line. (E–G) Transfection of Myc-tagged FERM domain had a dominant-negative effect causing elongation of spines in 14DIV wild-type neurons (E). (F) Cumulative plot of the length of dendritic protrusions. (G) Quantification of density of dendritic protrusions ($p > 0.05$). Data are presented as mean \pm SEM. Scale bar, (A, D, and E) 5 μ m.

immunoprecipitates. The EGFP-KCC2-CTD was only found in immunoprecipitates of extracts from cells expressing the FERM domain of 4.1N. Hence, the FERM domain but not the SABD or CTD of 4.1N is critical in mediating the interaction between KCC2 and 4.1N (Figure 6F). Furthermore, the distribution of endogenous KCC2 in primary cultured neurons is very similar to that of endogenous 4.1N (Figure S5), and, in line with this, there was a clear colocalization of Myc-tagged KCC2 and 4.1N in dendritic spines (Figures 7A–7D).

Both KCC3-FL and KCC3-CTD failed to mimic the effect of the corresponding KCC2 constructs, indicating that KCC3 is not able to interact with the spine proteins that are important for the morphogenic role of KCC2 (see Figures 3 and 4). Indeed, the pull-down assay showed that KCC3 does not interact with the 4.1N FERM domain (Figure 6G).

We then transfected the Myc-tagged FERM domain of 4.1N into WT neurons and examined their dendritic protrusion morphology. Strikingly, this resulted in a spine phenotype (length: $2.86 \pm 0.17 \mu$ m; $n = 1150$; 15 neurons; density of protrusions: $10.25 \pm 0.82/\mu$ m; $n = 54$ dendrites; Figures 7E–7G) that was similar to what was found in both the $KCC2^{-/-}$ neurons (see Figure 1) and following transfection of the WT neurons with KCC2-CTD (see Figure 5). No significant difference in the total dendritic length (WT: 411.2 ± 58.1 ; $KCC2^{-/-}$: 387.8 ± 68.5 ; FERM: 415.6 ± 88 ; $p = 0.66$

ANOVA; $n = 9$) and branching (WT: 7.77 ± 1.64 ; $KCC2^{-/-}$: 7.11 ± 1.69 ; FERM: 6.89 ± 1.45 ; $p = 0.49$ ANOVA; $n = 9$) was observed between WT, $KCC2^{-/-}$, and WT neurons expressing the 4.1N FERM domain. It is obvious that, while FERM might have multiple roles based on interactions with other spine proteins, our findings are consistent with the conclusion that a dominant-negative function of the Myc-tagged FERM domain is involved in the inhibition of the interaction between 4.1N and the KCC2-CTD.

DISCUSSION

A major observation in our work is that KCC2, a member of the cation-chloride cotransporter family, has an effect on neuronal morphology that is mediated by protein-protein interactions at the level of the cytoskeleton. In particular, we demonstrate a crucial role for KCC2 in dendritic spine formation, which is independent of the well-established function of KCC2 as the major neuron-specific K-Cl cotransporter (Hübner et al., 2001; Payne et al., 1996, 2003; Rivera et al., 1999; Woo et al., 2002). We also show that the C-terminal domain of KCC2 is directly interacting with the cytoskeletal protein 4.1N.

The compromised development of spines in $KCC2^{-/-}$ neurons was obvious in the light of both structural and functional data. Most of the spines in the $KCC2^{-/-}$ neurons were remarkably long when compared to those in

the WT neurons. The morphologically aberrant $KCC2^{-/-}$ spines had a “filopodia-like” appearance after about 2 weeks in culture, at a time point when the WT neurons had developed morphologically mature spines. In line with this, only a minor fraction of dendritic protrusions in $KCC2^{-/-}$ neurons were positive for the postsynaptic marker PSD-95, indicating a decreased number of excitatory synapses. Furthermore, double immunostainings with the presynaptic marker VGLUT1 and the postsynaptic markers PSD-95 and HOMER showed a significant reduction in synaptic clusters in the $KCC2^{-/-}$ cultures. At the functional level, we found a pronounced decrease in presynaptic destaining of SynaptoRed (Betz et al., 1992), indicating a lower number of functional synapses, and, in agreement with this, the frequency of mEPSCs in $KCC2^{-/-}$ neurons was much lower than in the WT.

A key finding in the present work is that the spine phenotype could be rescued by transfecting the $KCC2^{-/-}$ neurons not only with full-length KCC2 (KCC2-FL) but also by the N-terminal domain deletion construct (KCC2- Δ NTD), which is not capable of mediating K-Cl cotransport as verified in both electrophysiological experiments in $KCC2^{-/-}$ neurons (cf. Khirug et al., 2005) and in ^{86}Rb flux assays in HEK293 cells (cf. Williams and Payne, 2004). KCC2- Δ NTD was not only able to restore the mature-like morphology of dendritic spines but also the number of functional synapses as shown by the significantly higher number of PSD-95-positive protrusions and the parallel increase in the frequency of mEPSCs in transfected $KCC2^{-/-}$ neurons. These findings are consistent with the conclusion that the role of KCC2 in spine maturation is not based on K-Cl cotransport but rather on KCC2 interactions with spine cytoskeletal proteins.

In order to gain information on the putative interacting partners of KCC2, we screened a number of proteins enriched in spines, including GluR1–4, PSD-95, GRIP, CaMKII, CRIP1, SAP97, and 4.1N (Kennedy et al., 2005; Niethammer et al., 1998; Shen et al., 2000), using KCC2 immunoprecipitation assays from adult mouse brain homogenate. The data we obtained point to 4.1N protein as a direct link between the C-terminal domain of KCC2 and the spine cytoskeleton. This is an exciting observation because 4.1N is generally thought to have a key role in mediating structural interactions between the cytoskeleton, transmembrane proteins, and adhesion molecules (Hoover and Bryant, 2000). Notably, the actin-rich cytoskeleton is critical for spinogenesis and also for the maintenance and plasticity of mature synapses (Halpain, 2000; Matus, 2000; Yuste and Bonhoeffer, 2004; Segal, 2005). Both KCC2 and 4.1N are abundant in neurons during early development at the time of synaptogenesis, and their expression is steeply correlated with the maturation of excitatory synapses (Gulyas et al., 2001; Ludwig et al., 2003; Rivera et al., 1999; Walensky et al., 1999). The dominant-negative effect of both the KCC2-CTD and 4.1N-FERM constructs, resulting in a dendritic protrusion phenotype that mimics the one found in $KCC2^{-/-}$ neurons, provides further evidence for KCC2 as a scaffold

molecule in dendritic spines. The present results do not, of course, exclude additional mechanisms based on interactions of KCC2 with other intracellular molecules involved in the regulation of spine morphology.

The conclusion that KCC2 has a role in spine formation also under in vivo conditions is supported by the data from neurons in acute slices from the $KCC2^{hy/null}$ mice, which have a reduction of >80% in KCC2 protein level (Tornberg et al., 2005). As could be expected, the increase in the length of dendritic protrusions in the $KCC2^{hy/null}$ neurons was not as pronounced as in cultured $KCC2^{-/-}$ neurons. Here, it is also important to note that the spine morphology in the $KCC2^{-/-}$ organotypic cultures was similar to the one found in primary $KCC2^{-/-}$ cultures.

The present work does not, of course, imply that the role of KCC2 in the morphological maturation of neurons is restricted to the mechanisms of spine formation at the level of protein-protein interactions. The depolarizing actions of GABA that take place in immature neurons at a developmental stage where KCC2 expression is absent or low have been shown to exert various kinds of trophic effects (Owens and Kriegstein, 2002; Represa and Ben-Ari, 2005). Interestingly, a recent in vivo study by Cancedda et al. (2007) demonstrated that eliminating the depolarizing action of GABA by premature expression of KCC2 in immature ventricular progenitors and in cortical neurons derived thereof resulted in a marked disturbance of dendritic development. This action was dependent on the functionality of KCC2 as a K-Cl cotransporter, as shown by pharmacological data and by parallel experiments involving overexpression of an inward-rectifying K^+ channel that lowered the resting membrane potential and mimicked the effects of KCC2. In this context, it is relevant to point out that in the present work we did not observe differences in the morphological parameters of the dendritic tree between the WT and $KCC2^{-/-}$ neurons. This finding (and the data described above) indicates that the aberrant morphology of the dendritic spines of the $KCC2^{-/-}$ neurons is not attributable to abnormal dendritic development.

Spine morphology and the expression levels of KCC2 are known to undergo both long-term and short-term changes during neuronal development, plasticity, epileptic activity, and damage (Matus, 2000; Payne et al., 2003; Rivera et al., 2002, 2004; Zhou et al., 2004; Segal, 2005). The present findings are likely to pave the way for new approaches in studies of the mechanisms underlying the interactions that take place between KCC2 and the cytoskeleton in spine morphogenesis under these conditions. Finally, our work points to a novel aspect of synaptic homeostasis during neuronal maturation. In this scenario, the progressive developmental increase in the number of functional glutamatergic synapses that target spines will be paralleled by an increase in the KCC2-dependent neuronal Cl^- extrusion capacity (Gulyas et al., 2001; Khirug et al., 2005) and consequently by an increase in the efficacy of GABAergic inhibition (Payne et al., 2003). Thus, KCC2 may function as a synchronizing factor in the development of inhibitory and excitatory neurotransmission.

EXPERIMENTAL PROCEDURES

Experimental Animals

Generation of the KCC2 null allele and genotyping of the mice have been described previously (Vilen et al., 2001). Heterozygote (*KCC2*^{+/-}) females and heterozygote males were crossed to produce *KCC2*^{-/-} embryos. All animal experiments were approved by the ethics committee for animal research at the University of Helsinki. Generation and genotyping of *KCC2*^{hy/nnull} compound heterozygous mice, which retain 17% ± 5% of normal KCC2 protein levels in the brain, have been described previously (Tomberg et al., 2005). Briefly, one allele harbors the null mutation (a *neo*-cassette in exon 4 of the *KCC2* gene), and the other allele is hypomorphic (a *neo*-cassette within intron 3 in the opposite orientation relative to the *KCC2* gene).

Primary Cultures

We used day 16 embryos in this study for primary neuronal culture. Cortex from each littermate was dissected and plated separately. Neurons were grown on coverslips coated with poly-DL-ornithine at a density of 0.2 × 10⁶ cells/coverslip in Neurobasal medium supplemented with B27 (GIBCO, Life Technologies). In some experiments, 2 μM TTX and bicuculline (10 μM) were added to the culture medium. Genotyping was carried out after plating. Cultures from WT littermates were used as controls.

Biocytin Loading of Acute and Organotypic Slices

Acute slices were cut from postnatal day 16 (P16) mice brains using standard methods. Briefly, the brain was quickly dissected in ice-cold solution containing (in mM) NaCl, 124; KCl, 3; NaH₂PO₄, 1.25; MgSO₄, 10; NaHCO₃, 26; D-glucose, 15; and CaCl₂, 1.0; equilibrated with 5% CO₂/95% O₂. 400 μm thick slices were cut sagittally in the above solution, and stored for 1–4 hr at room temperature in a solution containing (in mM) NaCl, 124; KCl, 3; NaH₂PO₄, 1.25; MgSO₄, 1; NaHCO₃, 26; D-glucose, 15; CaCl₂, 2.0; and 5% CO₂/95% O₂.

For cortical organotypic cultures (Stoppini et al., 1991), E19 slices were cut and placed on sterile Millicell-CM membranes (Millipore, Bedford, MA, USA) in 6-well culture trays with 1 ml Neurobasal medium containing B27 supplement (GIBCO, Life Technologies), penicillin (100 units/ml), and streptomycin (100 μg/ml). The medium was changed the next day for Neurobasal medium containing B27 supplement and maintained at 37°C under 5% CO₂ in air for 2 weeks. Half the medium was replaced every 3 days.

For biocytin loading, slices were placed in a submerged recording chamber and perfused with the extracellular solution supplemented with picrotoxin (100 μM), D-AP-5 (50 μM), and TTX (1 μM), at 32°C. Visually identified neurons were recorded with patch electrodes (2–4 MΩ) in the whole-cell mode (holding voltage -70 mV) containing (in mM) CsMeSO₄, 130; HEPES, 10; EGTA, 0.5; Mg-ATP, 4; Na-GTP, 0.3; QX-314, 5; NaCl, 8; and biocytin, 10; 285 mOsm, pH 7.2. After at least 15 min, the electrode was slowly removed, and the slices were fixed in 4% PFA in PBS. Biocytin was visualized using Alexa 488-Avidin (Molecular Probes).

DNA Constructs and Transfection

Constructs used for transfection: rat KCC2 full-length (GenBank: U55816), KCC2-CTD (aa 637–1116), and KCC2-ΔNTD with N-terminal deletion (aa 1–100) were cloned into the pEGFP-IRES vector for bicistronic expression of KCC2 and EGFP (Quattromed Ltd). EGFP-KCC2-CTD, EGFP-KCC2-ΔCTD (aa 1–793), and EGFP-KCC3-CTD (aa 722–1150) fusion constructs were made using the EGFP-C1 vector (Clontech). The KCC3-FL (GenBank: NM 133649) construct in pCI-neo was a gift from Dr. Christian Hübner. Rat Myc-tagged 4.1N was inserted into the mammalian expression vector pcDNA3.1 (Invitrogen). The expression vectors for three domains of 4.1N (FERM, 97–378; SABD, 461–576; CTD, 633–879; GenBank: NM 172090) were generated using the polymerase chain reaction (PCR) with appropriate oligonucleotides.

Transfection of DNA constructs was carried out using the calcium phosphate method. The culture medium was replaced by 500 μl pre-warmed Neurobasal containing 10 mM Mg²⁺ 1 hr before adding transfection mixture. For calcium phosphate precipitation, the solution in each well in a 24-well plate (35 μl) contained 2 μg DNA, 0.25 M CaCl₂ mixed with 17.5 μl 2xHeBS (274 mM NaCl, 10 mM KCl, 1.4 mM Na₂HPO₄, 15 mM D-glucose, and 42 mM HEPES). Cells were incubated at 37°C in 5% CO₂ for 2–4 hr. After a fine precipitate was observed on top of the cells, they were washed with Neurobasal medium containing 10 mM Mg²⁺. Thereafter, the original culture medium was applied. Transfection using lipofectamin 2000+ was performed following the instructions from the supplier (Invitrogen). The functionality of each construct was verified in HEK293 cells using western blot analysis. Transfections were done at 9DIV if not otherwise stated, and all experiments were carried out at 14DIV.

Fluorescence Imaging of Active Synaptic Terminals

Active synaptic terminals on cultured neurons were visualized using a styryl dye-loading procedure. SynaptoRed C2 was purchased from Sigma. The composition of the standard extracellular solution was (in mM) 127 NaCl, 3 KCl, 2 CaCl₂, 1.3 MgCl₂, 10 D-glucose, and 20 HEPES, pH 7.4 was adjusted with NaOH. Cells were exposed for 1 min to high K⁺ solution (50 mM; Na⁺ lowered accordingly) containing SynaptoRed C2 (15 μM) and then washed with standard extracellular solution for at least 20 min. An image of SynaptoRed-loaded terminals was obtained upon washout using CellR video-imaging system (Olympus Biosystems). Subsequently, destaining of the terminals with high K⁺-containing solution (1 min) was performed, and a second image was obtained and subtracted from the first one. The resulting image corresponds to active synaptic terminals (Betz et al., 1992). Bright fluorescent puncta of small size (diffraction-limited image of a point source) were counted as markers of individual presynaptic terminals.

Analysis of Excitatory Miniature Postsynaptic Currents

mEPSCs were recorded from primary cultured neurons (14–17DIV) in whole-cell voltage-clamp configuration at room temperature (23°C–25°C). The composition of the extracellular solution was (in mM) NaCl 124, KCl 3, CaCl₂ 2, NaH₂PO₄ 1.1, MgSO₄ 1.3, HEPES 20, D-glucose 10, bicuculline 0.01, and TTX 0.002. pH 7.4 was adjusted with NaOH. Patch pipettes were fabricated from borosilicate glass (Harvard Apparatus, UK), and their resistance ranged from 6 to 8 MΩ. The pipette solution consisted of (in mM) KCl 18, K-gluconate 111, CaCl₂ 0.5, BAPTA 5, Mg-ATP 2, HEPES 10, glucose 10, NaOH 2, pH 7.3 was adjusted with KOH. Membrane potential was clamped at -65 mV. Only cells with access resistance that did not exceed 20 MΩ were accepted for analysis. The average frequency and amplitude of these events were analyzed using the MiniAnalysis Program, version 5.6.6 (Synaptosoft). All measurements and analyses were made blind to genotype.

Measurement of the Efficacy of KCC2-Mediated Cl⁻ Extrusion in Neurons

KCC2-mediated Cl⁻ extrusion was quantified in cultured neurons as previously described (Khurug et al., 2005). Somatic recordings in standard extracellular solution at room temperature (22°C–24°C) were done in the whole-cell voltage-clamp configuration using a patch-clamp amplifier (EPC 10, HEKA Elektronik). Borosilicate glass patch pipette resistances ranged from 6.5 to 7.5 MΩ. Composition of the patch pipette solution was (in mM) 18 KCl, 111 K-gluconate, 0.5 CaCl₂, 2 NaOH, 10 glucose, 10 HEPES, and 2 Mg-ATP, 5 BAPTA, pH 7.3 (KOH). For local photolysis of the CNB-caged GABA compound (2 mM; Molecular Probes), 25 ms flashes from a UV laser (Enterprise 653, Coherent) were delivered via a multimode optical fiber through the objective. The diameter of the uncaging spot was ~10 μm. GABA was photolyzed at the soma and along the dendrite of a given neuron. NKCC1 was blocked throughout the experiments with 10 μM bumetanide, action potentials with 1 μM TTX, and GABA_B

receptors with 1 μ M CGP 55845. Under these conditions, the somatodendritic gradient of E_{GABA} provides a quantitative estimate of the efficacy of KCC2-mediated Cl^- extrusion (Khiring et al., 2005).

⁸⁶Rb Flux Assay of K-CI Cotransporter Activity in HEK293 Cells

⁸⁶Rb flux assays of the functionality of KCC2-FL and KCC2- Δ NTD were performed at room temperature on 1 day postconfluent HEK293 cells (Williams and Payne, 2004). Two days before the measurements, the cells were transfected with KCC2-FL, KCC2- Δ NTD, and EGFP constructs. The cells were washed three times in the control medium (135 mM NaCl, 5 mM RbCl, 1 mM $CaCl_2$, 1 mM $MgCl_2$, 1 mM Na_2HPO_4 , 2 mM Na_2SO_4 , 3 mM glucose, 15 mM HEPES, pH 7.4 and 0.1 mM ouabain). This was followed by 30 min preincubation in control medium in the presence or absence of 2 mM furosemide and/or 1 mM NEM. The cells were then exposed in the same medium for 4 min to 2 μ Ci/ml ⁸⁶RbCl. ⁸⁶Rb influx was terminated by five washes with ice-cold control flux medium containing 2 mM furosemide. Cells were solubilized in 2% SDS and assayed for ⁸⁶Rb by scintillation counting (1450 Microbeta, Wallac).

Image Acquisition and Quantification

Fluorescence images were acquired with a Leica TCS SP2 confocal microscope using an HCXPL APO 63 \times /1.4–0.6 oil or HC PL APO 20 \times /0.7 Imm Corr (water, glycerol, oil) objectives. Image stacks were 3D-deconvoluted using the Autoquant X software (Media Cybernetics Inc.) and viewed as maximal-intensity projections.

For time-lapse analysis 4D (x, y, z, t) image stacks were processed and analyzed using the Imaris 4 software (Bitplane) as previously described by Nagerl et al. (2004). Briefly, individual image stacks were spatially filtered by an edge-preserving algorithm, rescaled, and subtracted for baseline. To facilitate overview of the figures, the 3D stacks were volume rendered as 2D images using the blending projection view in Imaris.

Neurites were traced and quantified in 2D images with the NeuronJ software (Meijering et al., 2004; <http://rsb.info.nih.gov/ij/>). All morphometric, pre- and postsynaptic cluster analysis, and fluorescence intensity measurements were made blind to genotype and transfection with Imaris 4 software (Bitplane) and Image-Pro PLUS 4 analysis software (Media Cybernetics Inc.). The length of dendritic protrusions was measured from the dendritic shaft to the most distal point of the protrusions. For analysis of pre- and postsynaptic clusters the ImarisColoc feature in the Imaris 4 software was used.

Immunoprecipitation and Antibodies

The methods for immunoprecipitation from adult mouse brain homogenates and the HEK293 cell extract have been described previously (Cai et al., 2002). Transfected HEK293 cells or adult mouse brains were homogenized in ten volumes of TNE buffer (1% Nonidet P-40, 50 mM Tris-HCl, pH 8.0, 140 mM NaCl, 5 mM EDTA, 1 mM NaF, 1 mM Na_3VO_4 , 1 mM PMSF, 10 μ g/ml each of aprotinin and leupeptin). Thereafter, Triton X-100 was added to a final concentration of 1% (w/v), and the suspension was mixed at +4°C for 2 hr followed by centrifugation at 20,000 \times g for 20 min. Aliquots of 1 ml supernatant preclarified by GammaBind G-Sepharose (Amersham Biosciences) were incubated with the appropriate IgG (2 μ g) or antiserum (2 μ l) overnight at +4°C; thereafter, 20 μ l of GammaBind G-Sepharose was added, and the incubation was continued with gentle rotation for 2 hr. GammaBind-Sepharose beads were washed for 5 \times 20 min with TNE buffer and 2 \times 10 min with PBS and finally eluted in 20 μ l of SDS sample buffer, heated 5 min at +95°C, and centrifuged briefly. The supernatants and 10 μ g lysate (input) from brain tissue or HEK293 cells were separated by SDS-PAGE. The gels were transferred to nitrocellulose membrane and immunoblotted with the appropriate antibodies. Blots were developed by using the ECL Plus (Amersham Biosciences).

Anti-KCC2-CTD (Ludwig et al., 2003) and anti-4.1N antibodies were produced in the laboratory (see Figure S6). Other antibodies used were anti-KCC2-NTD (Blaesse et al., 2006), anti-Myc (Sigma), anti-GFP (BD Bioscience), anti-PSD-95 (Upstate Biotech), anti-GluR1 (Cai et al., 2002), anti-GluR-4 (Coleman et al., 2003), anti-GRIP (Upstate Biotech), anti-CaMKII (Santa Cruz), Alexa-488- (Molecular Probes), and anti-Mouse (or rabbit) IgG-HRP-conjugated (Jackson Immuno Research) secondary antibodies. Control experiments showing the specificity of these antibodies are illustrated in Figure S4.

Production of the 4.1N-Specific Antibody

A specific antiserum against 4.1N was generated by immunizing New Zealand White rabbits with purified GST fusion protein of rat 4.1N C-terminal domain (residues 733–879; GenBank: NM 172090). Immunization (primary immunization with 300 μ g protein; two boosters, 200 μ g each) and collection of sera were performed according to standard protocols in the Animal Facility of the Viikki Biocenter, University of Helsinki. For characterization of the 4.1N antibody, see Figure S6.

Biotinylation of Cell-Surface Proteins

48 hr after transfection, cells were placed on ice and washed three times with ice-cold PBS. After the last wash, cold PBS was added containing 150 nM of biotin-sulfo-NHS (Sigma) and applied on ice for 90 min. Cells were rinsed three times with PBS, collected and homogenized in ST buffer (1% Triton X-100, 0.1% SDS, 1 mM EDTA, 50 mM NaCl, 20 mM Tris-HCl, pH 7.5, protease inhibitors). The lysate was centrifuged for 20 s and the supernatant precipitated with Streptavidin-sepharose (Sigma) by overnight incubation at +4°C. The precipitate was collected by a brief centrifugation and washed with PBS. Then the precipitate and 10 μ g cell lysate (input) were subjected to SDS-PAGE and western blotting with KCC2 antibody.

Statistical Analysis

Statistical analyses were performed using Origin software (Microcal) and Excel (Microsoft). Averaged data are presented as mean \pm standard error of the mean (SEM). Statistical significance was assessed using Student's unpaired t test and ANOVA. For morphological analysis of dendritic protrusions, the statistical significance was analyzed by the Kolmogorov-Smirnov test.

Supplemental Data

The Supplemental Data for this article can be found online at <http://www.neuron.org/cgi/content/full/56/6/1019/DC1/>.

ACKNOWLEDGMENTS

We thank Dr. H.G. Nothwang for providing the KCC2 N-terminal antibody. We also thank K. Tanhuanpää and M. Molin for help with microscopy and image processing, Timo Päiverinta for help with the figure graphics, as well as M. Heikura and M. Palviainen for excellent technical support. This work was supported by grants from the Academy of Finland to K.Kaila, M.S.A., M.S., C.R., K. Keinänen, and L.K.; Sigrid Juselius Foundation and Biocentrum Helsinki to K. Kaila, M.S.A., M.S., and C.R.; the Finnish Graduate School in Neuroscience to C.C., H.L., and A.L.; the Finnish Cultural Foundation to S.K.; and the Deutsche Akademische Austauschdienst to P.B. K. Kaila is a member of the Nordic Center of Excellence, WIRED.

Received: February 13, 2007

Revised: June 21, 2007

Accepted: October 30, 2007

Published: December 19, 2007

REFERENCES

- Akerman, C.J., and Cline, H.T. (2006). Depolarizing GABAergic conductances regulate the balance of excitation to inhibition in the developing retinotectal circuit *in vivo*. *J. Neurosci.* 26, 5117–5130.
- Adragna, N.C., Fulvio, M.D., and Lauf, P.K. (2004). Regulation of K-Cl cotransport: from function to genes. *J. Membr. Biol.* 3, 109–137.
- Ben-Ari, Y. (2002). Excitatory actions of gaba during development: the nature of the nurture. *Nat. Rev. Neurosci.* 9, 728–739.
- Bennett, V. (1989). The spectrin-actin junction of erythrocyte membrane skeletons. *Biochim. Biophys. Acta* 1, 107–121.
- Bennett, V., and Baines, A.J. (2001). Spectrin and ankyrin-based pathways: metazoan inventions for integrating cells into tissues. *Physiol. Rev.* 3, 1353–1392.
- Betz, W.J., Mao, F., and Bewick, G.S. (1992). Activity-dependent fluorescent staining and destaining of living vertebrate motor-nerve terminals. *J. Neurosci.* 2, 363–375.
- Blaesse, P., Guillemain, I., Schindler, J., Schweizer, M., Delpire, E., Khiroug, L., Friauf, E., and Nothwang, H.G. (2006). Oligomerization of KCC2 correlates with development of inhibitory neurotransmission. *J. Neurosci.* 26, 10407–10419.
- Cai, C., Coleman, S.K., Niemi, K., and Keinanen, K. (2002). Selective binding of synapse-associated protein 97 to GluR-A alpha-amino-5-hydroxy-3-methyl-4-isoxazole propionate receptor subunit is determined by a novel sequence motif. *J. Biol. Chem.* 277, 31484–31490.
- Cancedda, L., Fiumelli, H., Chen, K., and Poo, M.M. (2007). Excitatory GABA action is essential for morphological maturation of cortical neurons *in vivo*. *J. Neurosci.* 27, 5224–5235.
- Casula, S., Shmukler, B.E., Wilhelm, S., Stuart-Tilley, A.K., Su, W.F., Chernova, M.N., Brugnara, C., and Alper, S.L. (2001). A dominant negative mutant of the KCC1 K-Cl cotransporter - both N- and C-terminal cytoplasmic domains are required for K-Cl cotransport activity. *J. Biol. Chem.* 45, 41870–41878.
- Coleman, S.K., Cai, C., Mottershead, D.G., Haapalahti, J.P., and Keinanen, K. (2003). Surface expression of GluR-D AMPA receptor is dependent on an interaction between its C-terminal domain and a 4.1 protein. *J. Neurosci.* 3, 798–806.
- Chudotvorova, I., Ivanov, A., Rama, S., Hübner, C.A., Pellegrino, C., Ben-Ari, Y., and Medina, I. (2005). Early expression of KCC2 in rat hippocampal cultures augments expression of functional GABA synapses. *J. Physiol.* 566, 671–679.
- Denker, S.P., and Barber, D.L. (2002). Ion transport proteins anchor and regulate the cytoskeleton. *Curr. Opin. Cell Biol.* 2, 214–220.
- Ethell, I.M., and Pasquale, E.B. (2005). Molecular mechanisms of dendritic spine development and remodeling. *Prog. Neurobiol.* 3, 161–205.
- Freund, T.F., and Buzsáki, G. (1996). Interneurons of the hippocampus. *Hippocampus* 4, 347–470.
- Ganguly, K., Schinder, A.F., Wong, S.T., and Poo, M. (2001). GABA itself promotes the developmental switch of neuronal GABAergic responses from excitation to inhibition. *Cell* 105, 521–532.
- Gulyas, A.I., Sik, A., Payne, J.A., Kaila, K., and Freund, T.F. (2001). The KCl cotransporter, KCC2, is highly expressed in the vicinity of excitatory synapses in the rat hippocampus. *Eur. J. Neurosci.* 12, 2205–2217.
- Halpain, S. (2000). Actin and the agile spine: how and why do dendritic spines dance? *Trends Neurosci.* 4, 141–146.
- Hering, H., and Sheng, M. (2001). Dendritic spines: structure, dynamics and regulation. *Nat. Rev. Neurosci.* 12, 880–888.
- Hoover, K.B., and Bryant, P.J. (2000). The genetics of the protein 4.1 family: organizers of the membrane and cytoskeleton. *Curr. Opin. Cell Biol.* 2, 229–234.
- Hübner, C.A., Stein, V., Hermans-Borgmeyer, I., Meyer, T., Ballanyi, K., and Jentsch, T.J. (2001). Disruption of KCC2 reveals an essential role of K-Cl cotransport already in early synaptic inhibition. *Neuron* 2, 515–524.
- Kennedy, M.B., Beale, H.C., Carlisle, H.J., and Washburn, L.R. (2005). Integration of biochemical signalling in spines. *Nat. Rev. Neurosci.* 6, 423–434.
- Khiroug, S., Huttu, K., Ludwig, A., Smirnov, S., Voipio, J., Rivera, C., Kaila, K., and Khiroug, L. (2005). Distinct properties of functional KCC2 expression in immature mouse hippocampal neurons in culture and in acute slices. *Eur. J. Neurosci.* 21, 899–904.
- Kim, E., and Sheng, M. (2004). PDZ domain proteins of synapses. *Nat. Rev. Neurosci.* 5, 771–781.
- Kirov, S.A., Goddard, C.A., and Harris, K.M. (2004). Age-dependence in the homeostatic upregulation of hippocampal dendritic spine number during blocked synaptic transmission. *Neuropharmacology* 5, 640–648.
- Kubota, Y., Hatada, S., Kondo, S., Karube, F., and Kawaguchi, Y. (2007). Neocortical inhibitory terminals innervate dendritic spines targeted by thalamocortical afferents. *J. Neurosci.* 27, 1139–1150.
- Lee, H., Chen, C.X.Q., Liu, Y.J., Aizenman, E., and Kandler, K. (2005). KCC2 expression in immature rat cortical neurons is sufficient to switch the polarity of GABA responses. *Eur. J. Neurosci.* 9, 2593–2599.
- Ludwig, A., Li, H., Saarma, M., Kaila, K., and Rivera, C. (2003). Developmental up-regulation of KCC2 in the absence of GABAergic and glutamatergic transmission. *Eur. J. Neurosci.* 12, 3199–3206.
- Matus, A. (2000). Actin-based plasticity in dendritic spines. *Science* 5492, 754–758.
- Meijering, E., Jacob, M., Sarria, J.C., Steiner, P., Hirling, H., and Unser, M. (2004). Design and validation of a tool for neurite tracing and analysis in fluorescence microscopy images. *Cytometry A* 58, 167–176.
- Nagerl, U.V., Eberhorn, N., Cambridge, S.B., and Bonhoeffer, T. (2004). Bidirectional activity-dependent morphological plasticity in hippocampal neurons. *Neuron* 5, 759–767.
- Niethammer, M., Valtschanoff, J.G., Kapoor, T.M., Allison, D.W., Weinberg, T.M., Craig, A.M., and Sheng, M. (1998). CRIPT, a novel postsynaptic protein that binds to the third PDZ domain of PSD-95/SAP90. *Neuron* 20, 693–707.
- Owens, D.F., and Kriegstein, A.R. (2002). Is there more to GABA than synaptic inhibition? *Nat. Rev. Neurosci.* 3, 715–727.
- Payne, J.A., Stevenson, T.J., and Donaldson, L.F. (1996). Molecular characterization of a putative K-Cl cotransporter in rat brain - A neuronal-specific isoform. *J. Biol. Chem.* 27, 16245–16252.
- Payne, J.A., Rivera, C., Voipio, J., and Kaila, K. (2003). Cation-chloride co-transporters in neuronal communication, development and trauma. *Trends Neurosci.* 4, 199–206.
- Pinder, J.C., Clark, S.E., Baines, A.J., Morris, E., and Gratzner, W.B. (1981). The construction of the red cell cytoskeleton. *Prog. Clin. Biol. Res.* 55, 343–361.
- Represa, A., and Ben-Ari, Y. (2005). Trophic actions of GABA on neuronal development. *Trends Neurosci.* 28, 278–283.
- Rivera, C., Voipio, J., Payne, J.A., Ruusuvuori, E., Lahtinen, H., Lamsa, K., Pirvola, U., Saarma, M., and Kaila, K. (1999). The K⁺/Cl⁻ co-transporter KCC2 renders GABA hyperpolarizing during neuronal maturation. *Nature* 397, 251–255.
- Rivera, C., Li, H., Thomas-Crusells, J., Lahtinen, H., Viitanen, T., Nanobashvili, A., Kokaia, Z., Airaksinen, M.S., Voipio, J., Kaila, K., and Saarma, M. (2002). BDNF-induced TrkB activation down-regulates the K⁺-Cl⁻ cotransporter KCC2 and impairs neuronal Cl⁻ extrusion. *J. Cell Biol.* 5, 747–752.
- Rivera, C., Voipio, J., Thomas-Crusells, J., Li, H., Emri, Z., Sipilä, S., Payne, J.A., Minichiello, L., Saarma, M., and Kaila, K. (2004).

- Mechanism of activity-dependent downregulation of the neuron-specific K-Cl cotransporter KCC2. *J. Neurosci.* **19**, 4683–4691.
- Rivera, C., Voipio, J., and Kaila, K. (2005). Two developmental switches in GABAergic signalling: the K⁺-Cl⁻ cotransporter KCC2 and carbonic anhydrase CAVII. *J. Physiol.* **562**, 27–36.
- Russell, J.M. (2000). Sodium-potassium-chloride cotransport. *Physiol. Rev.* **1**, 211–276.
- Scott, C., Bellamy, M.L., Hayes, N.V., and Baines, A.J. (1998). Distribution and activities of neuronal protein 4.1 isoforms. *Biochem. Soc. Trans.* **2**, S106.
- Scott, C., Keating, L., Bellamy, M., and Baines, A.J. (2001). Protein 4.1 in forebrain postsynaptic density preparations: enrichment of 4.1 gene products and detection of 4.1R binding proteins. *Eur. J. Biochem.* **4**, 1084–1094.
- Segal, M. (2005). Dendritic spines and long-term plasticity. *Nat. Rev. Neurosci.* **6**, 277–284.
- Shen, L., Liang, F., Walensky, L.D., and Huganir, R.L. (2000). Regulation of AMPA receptor GluR1 subunit surface expression by a 4.1-N-linked actin cytoskeletal association. *J. Neurosci.* **20**, 7932–7940.
- Sipila, S.T., Schuchmann, S., Voipio, J., Yamada, J., and Kaila, K. (2006). The cation-chloride cotransporter NKCC1 promotes sharp waves in the neonatal rat hippocampus. *J. Physiol.* **573**, 765–773.
- Somogyi, P., Tamas, G., Lujan, R., and Buhl, E.H. (1998). Salient features of synaptic organisation in the cerebral cortex. *Brain Res. Brain Res. Rev.* **2–3**, 113–135.
- Stoppini, L., Buchs, P.A., and Muller, D. (1991). A simple method for organotypic cultures of nervous-tissue. *J. Neurosci. Methods* **2**, 173–182.
- Tornberg, J., Voikar, V., Savilahti, H., Rauvala, H., and Airaksinen, M.S. (2005). Behavioural phenotypes of hypomorphic KCC2-deficient mice. *Eur. J. Neurosci.* **5**, 1327–1337.
- Vilen, H., Eerikainen, S., Tornberg, J., Airaksinen, M.S., and Savilahti, H. (2001). Construction of gene-targeting vectors: a rapid Mu in vitro DNA transposition-based strategy generating null, potentially hypomorphic, and conditional alleles. *Transgenic Res.* **1**, 69–80.
- Walensky, L.D., Blackshaw, S., Liao, D.Z., Watkins, C.C., Weier, H.U.G., Parra, M., Huganir, R.L., Conboy, J.G., Mohandas, N., and Snyder, S.H. (1999). A novel neuron-enriched homolog of the erythrocyte membrane cytoskeletal protein 4.1. *J. Neurosci.* **15**, 6457–6467.
- Williams, J.R., and Payne, J.A. (2004). Cation transport by the neuronal K(+)-Cl(-) cotransporter KCC2: thermodynamics and kinetics of alternate transport modes. *Am. J. Physiol. Cell Physiol.* **287**, C919–C931.
- Woo, N.S., Lu, J.M., England, R., McClellan, R., Dufour, S., Mount, D.B., Deutch, A.Y., Lovinger, D.M., and Delpire, E. (2002). Hyperexcitability and epilepsy associated with disruption of the mouse neuronal-specific K-Cl cotransporter gene. *Hippocampus* **2**, 258–268.
- Yamada, J., Okabe, A., Toyoda, H., Kilb, W., Luhmann, H.J., and Fukuda, A. (2004). Cl⁻ uptake promoting depolarizing GABA actions in immature rat neocortical neurones is mediated by NKCC1. *J. Physiol.* **557**, 829–841.
- Yamakawa, H., Ohara, R., Nakajima, D., Nakayama, M., and Ohara, O. (1999). Molecular characterization of a new member of the protein 4.1 family (brain 4.1) in rat brain. *Brain Res. Mol. Brain Res.* **70**, 197–209.
- Yuste, R., and Bonhoeffer, T. (2004). Genesis of dendritic spines: Insights from ultrastructural and imaging studies. *Nat. Rev. Neurosci.* **1**, 24–34.
- Zhou, Q., Homma, K.J., and Poo, M.M. (2004). Shrinkage of dendritic spines associated with long-term depression of hippocampal synapses. *Neuron* **44**, 749–757.